

HumanX: Toward Agile and Generalizable Humanoid Interaction Skills from Human Videos

Yinhuai Wang^{1,2*}, Qihan Zhao^{1*}, Yuen Fui Lau^{1*}, Runyi Yu¹, Hok Wai Tsui¹

Qifeng Chen^{1†}, Jingbo Wang^{2†}, Jiangmiao Pang², Ping Tan^{1†}

¹The Hong Kong University of Science and Technology ²Shanghai AI Laboratory

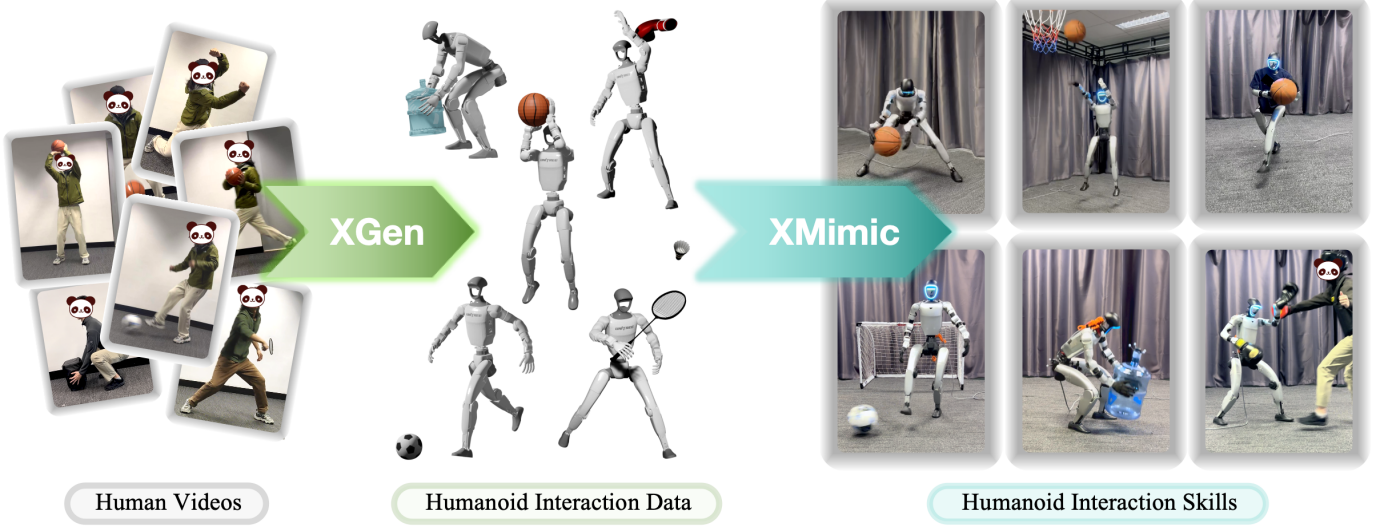


Fig. 1: HumanX enables diverse interaction skills through two core components. **XGen** synthesizes and augments humanoid interaction data from human video, which **XMimic** then uses to learn generalizable interaction skills. This results in autonomous interaction behaviors such as diverse basketball skills, consecutive football kicking, generalizable cargo pickup, and real-time counterattack against a human.

Abstract—Enabling humanoid robots to perform agile and adaptive interactive tasks has long been a core challenge in robotics. Current approaches are bottlenecked by either the scarcity of realistic interaction data or the need for meticulous, task-specific reward engineering, which limits their scalability. To narrow this gap, we present HumanX, a full-stack framework that compiles human video into generalizable, real-world interaction skills for humanoids, without task-specific rewards. HumanX integrates two co-designed components: XGen, a data generation pipeline that synthesizes diverse and physically plausible robot interaction data from video while supporting scalable data augmentation; and XMimic, a unified imitation learning framework that learns generalizable interaction skills. Evaluated across five distinct domains—basketball, football, badminton, cargo pickup, and reactive fighting—HumanX successfully acquires 10 different skills and transfers them zero-shot to a physical Unitree G1 humanoid. The learned capabilities include complex maneuvers such as pump-fake turnaround fadeaway jumpshots without any external perception, as well as interactive tasks like sustained human-robot passing sequences over 10 consecutive cycles—learned from a single video demonstration. Our experiments show that HumanX achieves over 8x higher generalization success than prior methods, demonstrating a scalable and task-agnostic pathway for learning versatile, real-world robot interactive skills. Page Link: <https://wyhuai.github.io/human-x/>

I. INTRODUCTION

Humanoid robots share a morphological affinity with humans, offering the potential to operate seamlessly in human

environments and interact with everyday objects. This inherent compatibility points to a vast, yet largely untapped resource: the rich diversity of skills demonstrated in human motion. However, unlocking this potential for robot learning remains a challenge. While behavior cloning (BC) offers a unified training paradigm, it relies on large-scale, costly teleoperated demonstrations [10, 4, 8]. Although reinforcement learning (RL) combined with physics simulation can substantially reduce the demand for large quantities of high-quality demonstrations, it usually requires meticulously engineered, task-specific reward functions, limiting its scalability across diverse tasks [11, 29, 15, 46, 64, 55]. Together, these bottlenecks have constrained the development of a general, scalable pipeline for acquiring humanoid interaction skills from human.

To address these limitations, we introduce HumanX, a full-stack framework that compiles human video into generalizable, real-world interaction skills for humanoids—without any task-specific reward design. HumanX integrates two synergistic, co-designed components: XGen, a data-generation pipeline that synthesizes diverse and physically plausible humanoid interaction data from monocular video while enabling scalable augmentation; and XMimic, a unified imitation-learning framework that acquires interaction skills purely by mimicking the behaviors synthesized by XGen.

A foundational insight behind XGen is that physically plau-

sible interactions are paramount for robot skill acquisition, far outweighing the need for photometrically faithful reconstructions. While estimating human and object motion separately from monocular video is well-studied [27, 39, 5, 51, 41], naively combining such independent estimates often yields physically implausible results due to issues like occlusion and depth ambiguity [12, 48]. XGen addresses this by fundamentally shifting the paradigm: it synthesizes interaction trajectories governed by physical priors, rather than pursuing exact reconstruction. This shift enables highly efficient data augmentation, allowing XGen to generate a broad distribution of physically consistent interaction trajectories from just a single video demonstration. Concretely, XGen operates in three stages: (1) extracting human motion and retargeting it to the robot; (2) physics-based synthesis of object trajectories coupled with contact-aware refinement; and (3) data augmentation through object geometry scaling and trajectory variation to maximize coverage for improved generalization.

Learning interaction skills by imitating human-object interaction (HOI) offers a task-agnostic paradigm [48, 50, 56]. However, deploying accurate, natural, and generalizable HOI skills on real humanoid robots remains a substantial challenge, due to the amplified complexity introduced by dynamic object interaction. XMimic addresses these challenges through four key innovations: (1) a unified reward scheme that enables accurate imitation of diverse, complex interaction behaviors; (2) a flexible perception scheme that can adapt to different real-world perception limitations; (3) generalization-first training via disturbed initialization and interaction-prioritized learning; and (4) scalable acquisition of multiple skill patterns from video. These components are integrated into a two-stage teacher-student framework, enabling a policy that achieves generalization far beyond the original video demonstrations and supports robust, flexible deployment.

We evaluate HumanX on 10 diverse loco-manipulation and interaction skills—spanning basketball, football, badminton, cargo handling, and robot-human fighting—on a Unitree G1 humanoid. The system demonstrates two practical deployment ways: (1) Without any explicit external sensing, it executes basketball skills including dribbling, layups, and complex pump-fake turnaround fadeaways, with an average success rate over 80%. (2) With object sensing from a MoCap system, it achieves sustained closed-loop interactions, including over 10 consecutive human-robot basketball passes and football kicks, along with reliable pickup of randomly placed objects. Notably, each skill is learned from a single video demonstration, highlighting the strong generalization capability of our approach. Beyond mimicry, the policies exhibit emergent, adaptive behaviors: if a human removes a carried object and sets it down, the robot autonomously walks to and regrasps it; during fighting, it distinguishes feints from real attacks and counters appropriately—demonstrating real-time interactive reasoning rather than simple motion replay. Quantitatively, HumanX achieves over 8x higher generalization success than prior methods, establishing a scalable, task-agnostic pathway for acquiring versatile interactive skills from human videos.

II. RELATED WORK

1) Data Acquisition for Humanoid Loco-Manipulation: Retargeting human motion to humanoids and applying reinforcement learning for imitation has shown significant promise for agile, dynamic skills [14, 13, 32, 22, 25, 65, 7, 19, 53, 40, 62, 59]. For instance, SFV [34] estimates human pose from monocular video and enables simulated humanoids to perform complex acrobatics. SkillMimic [50, 48] estimates both human and object motion from video to train diverse basketball skills in simulation. VideoMimic [1] estimates human-scene interaction data from video and enables real-world humanoid-scene interaction through imitation. Meanwhile, GMR [2] provides a general motion retargeting framework that maps human motion to various robot morphologies. Several recent methods explore retargeting human-object or human-scene interaction data to train loco-manipulation policies [58, 52, 46]. However, these methods either rely on high-quality human-object interaction data for retargeting, or they are challenged by occlusion and depth ambiguity when attempting to estimate accurate HOI data from monocular video—especially for intricate skills like a turnaround fadeaway jumpshot. Furthermore, these methods suffer from low data efficiency, making it challenging to collect enough samples for well-generalized policies. Our approach overcomes these limitations by extracting robot motion from human video and synthesizing humanoid-object interaction through physical rules. This data can be efficiently augmented for learning generalizable interaction skills.

2) Reinforcement Learning for Humanoid Robots: Reinforcement learning (RL) in physics simulation has emerged as a key paradigm for whole-body humanoid control [14, 13, 21, 25, 20, 15, 38, 57, 45, 3, 7]. Early RL approaches for humanoids largely focused on gait learning, typically requiring carefully designed task-specific reward functions [42, 16, 23, 24]. This reward-engineering paradigm has also proven effective for a variety of other tasks, such as getting up [15, 17], goalkeeping [36], and box carrying [46].

Inspired by the success of imitation learning in character animation [33, 35, 28, 54], retargeting human motion to humanoids and applying imitation rewards has enabled robots to acquire diverse locomotion skills—such as parkour [66, 63], martial arts [53], jumping [14, 18], and even generalizable whole-body motion tracking [59, 62, 6, 61, 22, 32]—through unified imitation rewards. Extending this imitation-based paradigm to interaction has seen initial progress in simulation. For example, Wang et al. [48, 50] introduced Human-Object Interaction (HOI) imitation, leveraging contact-graph and interaction imitation rewards to learn basketball and dexterous manipulation skills within a unified reward scheme. Xu et al. [56] scaled HOI imitation to large-scale cross-embodiment HOI datasets. Tesler et al. [43] achieves HOI imitation on large-scale whole-body dexterous manipulation.

Recent works bring HOI imitation to real-world humanoid robots face substantial challenges [52, 58]: kinematic differences between humans and robots, the difficulty of maintaining physical plausibility during HOI retargeting, the complex

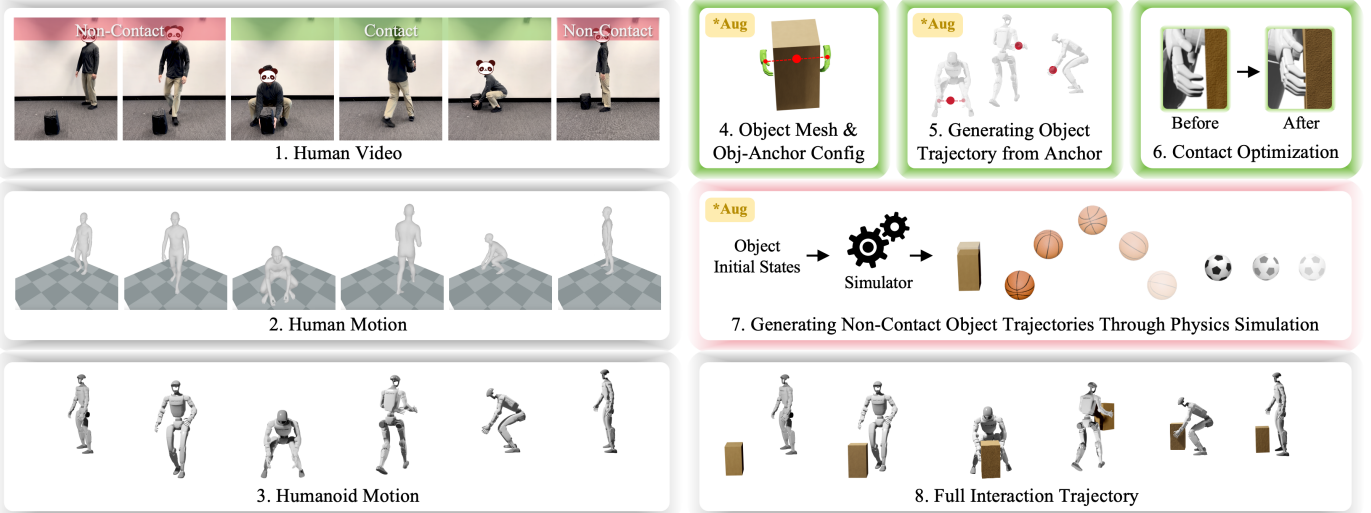


Fig. 2: Overview of XGen. The pipeline begins by estimating SMPL-based human motion from video and retargeting it to the humanoid’s morphology. The video is segmented into **contact** and **non-contact** phases. For the contact phase, a predefined anchor (e.g., the midpoint between the two palms) is used. The object mesh and its relative pose to the anchor are estimated from a keyframe (or defined manually). The object trajectory is then generated by transforming the object according to the anchor’s pose over time, followed by force-closure optimization to refine the robot poses. During the non-contact phases, diverse and physically plausible object trajectories are generated via simulation. Complete interaction trajectories are obtained by concatenating and smoothly interpolating the phases. Key steps supporting data augmentation—including object shape and trajectory variation—are highlighted in **yellow** in the figure.

sim-to-real gap introduced by object dynamics, and a tendency to overfit, resulting in poor generalization capability. Instead, our XGen and XMimic address these limitations effectively.

III. XGEN

XGen is a data synthesis pipeline that generates physically plausible humanoid interaction data from human demonstration videos. As illustrated in Fig. 2, it converts monocular human video into humanoid motion and synthesizes corresponding interaction under physical constraints. The pipeline further supports augmentation of object mesh, size, and trajectory to produce large-scale, diversified interaction data, laying a foundation for learning generalizable interaction skills. This section details the technical implementation of XGen.

A. Extracting Humanoid Motion from Human Video

Given a monocular RGB video with K frames, we first obtain an initial estimation of the 3D human pose sequence using GVHMR [39]. The estimated 3D human pose in the i -th frame is defined as:

$$\mathbf{h}_i = \left(\mathbf{h}_i^{\text{root}}, \mathbf{h}_i^{\text{joint}} \right), \quad i = 1, \dots, K, \quad (1)$$

where $\mathbf{h}_i^{\text{root}} \in \mathbb{R}^6$ represents the 6D pose (3D position and 3D orientation) of the human root, and $\mathbf{h}_i^{\text{joint}} \in \mathbb{R}^{J \times 3}$ denotes the 3D rotations of J SMPL [27] joints.

Subsequently, we use GMR [2] to retarget the human pose sequence into a pose sequence of the target humanoid robot, which involves three core steps: keypoint alignment, skeleton scaling, and IK-based optimization. After retargeting, the corresponding robot pose sequence is denoted as:

$$\mathbf{r}_i = \left(\mathbf{r}_i^{\text{root}}, \mathbf{r}_i^{\text{joint}} \right), \quad i = 1, \dots, K, \quad (2)$$

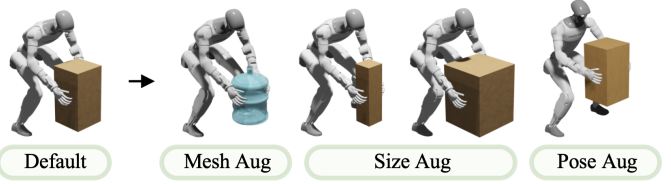


Fig. 3: Data Augmentation for Contact Phase.



Fig. 4: Data Augmentation for Non-Contact Phase.

where $\mathbf{r}_i^{\text{root}} \in \mathbb{R}^6$ is the 6D pose of the robot root, and $\mathbf{r}_i^{\text{joint}} \in \mathbb{R}^{N \times 1}$ represents the 1D rotations of N robot joints.

B. Synthesizing Humanoid-Object Interaction

We segment the data into contact and non-contact phases. In the contact phase, we leverage the invariance of the relative pose between a predefined anchor (e.g., the midpoint of the two palms) and the object. The object trajectory is synthesized by propagating this relative pose along the anchor trajectory derived from the robot motion sequence $\{\mathbf{r}_i\}$. The robot pose is then optimized under force-closure constraints to ensure physical plausibility during contact. For the non-contact phase, a physics simulator is used to generate physically consistent object trajectories.

As illustrated in Fig. 2, taking the example of box carrying, we first annotate the video frames into three sequential segments based on their timestamps t : a non-contact phase before contact begins ($t < t_s$), a contact phase ($t_s \leq t \leq t_e$), and a final non-contact phase after contact ends ($t > t_e$).

1) *The Contact Phase*: We consider the relative motion between a predefined anchor and the object as the core of an interaction. This representation exhibits favorable cross-embodiment properties, meaning the same anchor-object relationship can be transferred across different morphologies (e.g., from human to humanoid) while preserving interaction semantics. We primarily discuss two types of anchor definitions: (1) Using the midpoint between the two palms as the anchor, suitable for contact phases where the object is stably held with both hands, such as box carrying, shooting, and layups. (2) Using a specific body part as the anchor, suitable for contact phases involving a single-point interaction, such as hitting a shuttlecock or kicking a football ball.

Once the anchor is defined, we can estimate the object’s mesh and its rotation ϕ relative to the anchor at time t_s from the video frame \mathbf{v}_{t_s} using SAM-3D [5]. Alternatively, the mesh and the initial object-anchor pose can be manually defined, which also allows synthesizing interactions from videos where the object is not visibly present. The anchor’s trajectory is then derived from the robot motion sequence $\{\mathbf{r}_i\}$, and the corresponding object trajectory is obtained by preserving the relative transformation ϕ throughout the anchor’s motion.

To improve physical plausibility, the robot motion can be optimized frame-by-frame under force-closure constraints [26, 47, 49], yielding refined robot poses $\hat{\mathbf{r}}_t$ and corresponding object poses \mathbf{p}_t for each frame in the contact phase.

2) *The Non-Contact Phase*: To ensure smooth motion, linear interpolation is applied to the body poses over a window of k frames around the phase transition.

In the non-contact phase, object trajectories are synthesized using a physics simulator (e.g., IsaacGym [30]). Specifically: (1) After contact ends ($t > t_e$), the object is initialized in simulation with pose \mathbf{p}_{t_e} and a predefined initial velocity, and its trajectory is recorded under simulation. This applies to actions such as basketball shooting, football kicking, or object placement. (2) Before contact begins ($t < t_s$), —e.g., when catching a ball—we reverse the process: starting from \mathbf{p}_{t_s} , we simulate the object backward in time and then reverse the sequence to obtain the pre-contact trajectory. This allows accurate synthesis of motions such as a parabolic ball path into the hands. To ensure physical plausibility in the reversed simulation, object damping coefficients are inverted.

C. Interaction Augmentation

XGen supports data augmentation along multiple dimensions to increase the interaction diversity and data coverage.

1) *Scaling Object Geometry*: We apply scaling to the object mesh or replace it with a different geometry during the mesh acquisition stage. The subsequent XGen synthesis process ensures that interactions remain physically plausible with the scaled or substituted object. This allows generating data for

performing similar actions on different objects from a single demonstration video, as shown in Fig. 3.

2) *Enriching Object Trajectories in the Contact Phase*: The object trajectory within the contact phase can be augmented by applying simple geometric transformations—such as translation and scaling. The subsequent XGen pipeline ensures the physical plausibility of the interaction after augmentation. For example, from a single video demonstration of lifting a box, XGen can generate training data for lifting the same box from different heights, as illustrated in Fig. 3.

3) *Enriching Object Trajectories in the Non-Contact Phase*: We enrich the diversity of object trajectories in the non-contact phase by introducing parametric randomization to the object’s initial velocity in the physics simulation. For instance, from one demonstration of hitting a shuttlecock, XGen can produce data for hitting with different parabolic trajectories. Similarly, a single basketball shooting video can yield training data for making shots from various distances, as shown in Fig. 4.

IV. XMIMIC

XMimic is a unified interaction imitation learning framework that enables humanoid robots to acquire a wide repertoire of interaction skills from humanoid interaction data. To achieve accurate and natural imitation, strong generalization, and flexible deployment, we introduce key innovations across its training architecture, perception scheme, reward design, and simulation setup. In this section, we will go into detail about these technical aspects.

A. Teacher-Student Training Architecture

Our training process follows a two-stage teacher-student paradigm that first master individual skills with privilege information and then consolidate them into a unified deployable policy. The overall pipeline is illustrated in Fig. 5.

1) *Policy Formulation*: Given the observation \mathbf{s}_t as input, the policy output is parameterized as a Gaussian distribution:

$$\pi(\mathbf{a}_t | \mathbf{s}_t) \sim \mathcal{N}(\phi_\pi(\mathbf{s}_t), \Sigma_\pi), \quad (3)$$

where ϕ_π is a MLP that predicts mean of the action distribution. The covariance matrix Σ_π is learnable. The resulting action $\mathbf{a}_t \in \mathbb{R}^n$ (where n is the number of robot DoFs) is then transformed into joint torques via a PD controller.

2) *Training Privileged Teacher Policies*: Given n skill patterns and their corresponding datasets $\{\mathcal{D}_1, \dots, \mathcal{D}_n\}$ generated by XGen, we train a teacher policy π_{tea}^i on each dataset \mathcal{D}_i . The training procedure for a single teacher is as follows. A trajectory clip is sampled from its dedicated dataset, and the humanoid along with objects are initialized according to the first frame of the clip. At each timestep t , the policy receives a privileged state observation $\mathbf{s}_t = \{\mathbf{o}_t, \mathbf{o}_t^{\text{priv}}, \mathbf{s}_t^{\text{ext}}\}$, which comprises proprioception \mathbf{o}_t , privileged body information $\mathbf{o}_t^{\text{priv}}$, and object state $\mathbf{s}_t^{\text{ext}}$ (see Sec. IV-B for details). The policy then samples an action \mathbf{a}_t , which is executed in the physics simulator. Subsequently, the reward r_t (detailed in Sec. IV-C) is computed. The network parameters ϕ_π of the teacher policy are optimized using PPO [37] to maximize the expected cumulative reward.

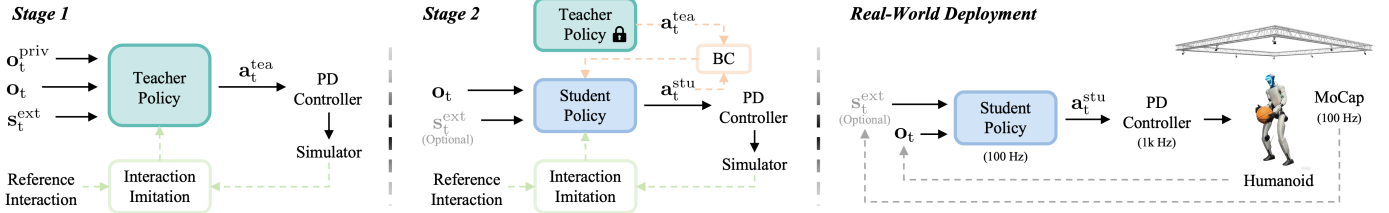


Fig. 5: XMimic follows a two-stage training pipeline. In the **Stage 1**, a teacher policy is learned with privileged state information under a unified interaction-imitation reward. In **Stage 2**, the teacher is distilled into a student policy that operates under realistic perceptual constraints, combining interaction imitation with behavior cloning. The resulting student policy can be deployed directly in real-world settings.

3) Distilling Teachers into a Deployable Student Policy:

The student policy is trained on the combined dataset $\mathcal{D} = \bigcup_i \mathcal{D}_i$ following similar procedure to the teacher, with two key distinctions. First, the student’s observation excludes all privileged state information, retaining only proprioception and optional object observations. Second, the training objective is extended to combine the PPO policy gradient term with a behavior cloning (BC) loss that distills knowledge from the pre-trained teachers:

$$\mathcal{L}_{\text{BC}} = \mathbb{E}_{(s, i) \sim \mathcal{G}} [\|\pi_{\text{stu}}(\mathbf{a} | s) - \pi_{\text{tea}}^i(\mathbf{a} | s)\|^2]. \quad (4)$$

B. Perception Design

1) *Perceiving External Force from Proprioception*: Inspired by the human ability to implicitly perceive interaction states through force feedback even without vision, we conducted a theoretical analysis demonstrating that humanoid robots can similarly infer external forces from proprioception. Specifically, the dynamics equation [9, 31] shows that external joint torques can be expressed as the difference between commanded torque and the sum of inertial, Coriolis, gravitational, and frictional components. In our real humanoid robot (Unitree G1), joint position \mathbf{q} and velocity $\dot{\mathbf{q}}$ are directly measurable, commanded torque τ_{cmd} is approximated from the PD controller, and acceleration information is implicitly provided via a history of velocity observations. The remaining terms are approximately constant. Consequently, our policy’s observation space (see the appendix) incorporates all relevant variables from this formulation, enabling force-aware interaction without dedicated force/torque sensors. The detailed dynamics equation derivation is provided in the appendix.

2) *Flexible Object Perception for Deployment*: XMimic supports two practical deployment schemes: a No External Perception (NEP) mode and a MoCap-based mode.

In *NEP mode*, object observations are removed during the student training, enabling the robot to rely solely on proprioception for dynamic interaction. This mode supports skills such as shooting, layups, dribbling, and complex maneuvers like pump-fake turnaround jumpshots. Its key advantage is that it requires no external sensors, making deployment simple and robust. However, this approach cannot handle non-contact interactions such as catching a flying ball.

In *MoCap mode*, the object observations are provided by a MoCap system. However, object tracking via MoCap often suffers from intermittent frame loss due to occlusion. To address this, our *MoCap mode* introduces realistically simulated



Fig. 6: Simulation Results on Basketball Catch-Shot. XMimic generalizes to novel ball-passing trajectories and target positions (green sphere) with accurate and natural interactions.

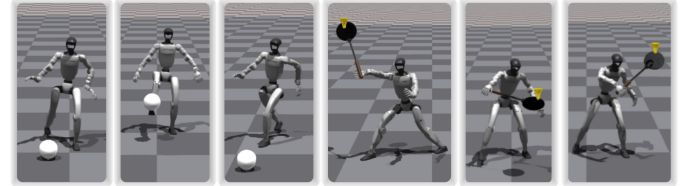


Fig. 7: Diverse Skill Patterns. XMimic supports learning multiple interaction patterns for a single skill, allowing the policy to autonomously select the most suitable pattern in response to object state. (Left): football-kicking patterns. (Right): badminton-hitting patterns.

frame loss into the object observations during the student training. This enables zero-shot adaptation to real-world MoCap streams with intermittent data loss.

C. Unified Interaction Imitation Reward

To enable accurate imitation of human-object interactions, we employ a composite reward $r_t = r_t^{\text{body}} + r_t^{\text{obj}} + r_t^{\text{rel}} + r_t^c + r_t^{\text{reg}}$. The body imitation reward r_t^{body} tracks body position, rotation, joint positions, and their velocities [14], and includes an adversarial motion prior (AMP) term for naturalness [35]. The object reward r_t^{obj} ensures accurate object state tracking. The relative motion reward r_t^{rel} encourages correct body-object relative spatial relationships, computed via relative position and rotation errors. The contact reward r_t^c penalizes deviations from the reference contact graph [48, 50], ensuring precise contact timing and location. The regularization term r_t^{reg} promotes motion smoothness and improve deployment stability.

D. Simulation Settings

1) *Disturbed Initialization*: To enhance the generalization of the learned interaction skills and prevent overfitting to the demonstration data, we apply random perturbations to the robot’s root rotation, root displacement, joint angles, as well as the object pose at the start of each training episode [60].

TABLE I: Main Simulation Results. SR, E_o , and E_h measure the success rate on the original data, the object position tracking error, and the key-body position tracking error, respectively, while GSR measures the success rate of skill generalization.

Method	Basketball Catch-Shot				Badminton Hitting				Cargo Pickup			
	SR \uparrow	GSR \uparrow	$E_o \downarrow$ (m)	$E_h \downarrow$ (cm)	SR \uparrow	GSR \uparrow	$E_o \downarrow$ (m)	$E_h \downarrow$ (m)	SR \uparrow	GSR \uparrow	$E_o \downarrow$ (cm)	$E_h \downarrow$ (cm)
SkillMimic [50]	0.0%	0.0%	1.25 (± 0.26)	10.3 (± 1.37)	68.2%	30.9%	2.94 (± 0.91)	0.48 (± 0.13)	0.4%	0.0%	25.1 (± 0.06)	28.3 (± 2.13)
OmniRetarget [58]	0.0%	0.0%	1.18 (± 0.15)	7.83 (± 0.95)	75.8%	20.4%	1.25 (± 1.15)	0.15 (± 0.10)	0.0%	0.0%	10.8 (± 0.00)	13.3 (± 1.57)
HDMI [52]	53.1%	2.4%	0.70 (± 0.11)	10.8 (± 2.41)	90.0%	25.3%	1.64 (± 0.66)	0.07 (± 0.02)	95.8%	1.8%	1.79 (± 0.22)	13.1 (± 1.28)
XMimic (Base)	93.4%	4.9%	0.69 (± 0.14)	6.36 (± 1.51)	97.1%	41.6%	1.32 (± 0.44)	0.12 (± 0.07)	100%	50.9%	1.56 (± 0.30)	6.58 (± 0.76)
+ DI	86.8%	13.5%	0.70 (± 0.08)	7.46 (± 0.46)	94.0%	60.5%	1.03 (± 0.57)	0.10 (± 0.05)	100%	94.5%	1.62 (± 0.03)	10.5 (± 1.23)
+ IT	93.4%	10.9%	0.83 (± 0.09)	6.97 (± 0.38)	100%	67.2%	1.33 (± 0.67)	0.10 (± 0.06)	99.6%	94.3%	1.51 (± 0.29)	9.62 (± 1.13)
+ Data Aug	77.6%	60.6%	0.76 (± 0.11)	8.34 (± 0.91)	100%	84.4%	0.98 (± 0.65)	0.10 (± 0.05)	/	/	/	/
+ Tea-Stu	86.8%	64.7%	0.85 (± 0.10)	7.83 (± 0.95)	100%	90.6%	0.90 (± 0.46)	0.09 (± 0.06)	99.3%	96.3%	1.38 (± 0.25)	8.67 (± 0.91)

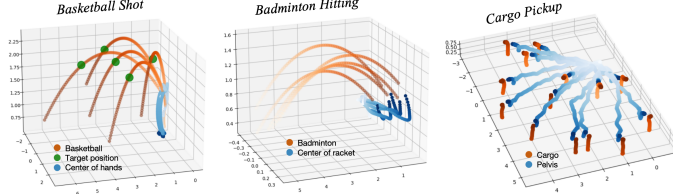


Fig. 8: Visualization of Generalization Performance in Simulation. With HumanX, skills learned from only **one video** generalize to unseen object positions, trajectories, and goals.

2) *Interaction Termination*: Additive reward formulations can lead the policy to converge toward local optima, such as learning body motion patterns while neglecting interaction-specific rewards [48]. To prioritize interaction learning, we propose Interaction Termination (IT). Specifically, when the reference frame involves a contact state, we monitor the relative position error between the object and predefined key bodies. If this error exceeds a threshold, the episode is terminated with probability. This probabilistic termination mechanism effectively prevents overfitting to restricted conditions and is crucial for achieving stable real-world deployment.

3) *Domain Randomization*: We apply domain randomization (DR) to various physical properties [44], including object size, mass, and coefficient of restitution, as well as robot friction coefficients, center of mass offsets, and perception noise. Additionally, we apply sustained random external forces to the robot during training. These DR terms are particularly important for achieving robust deployment.

V. ON GENERALIZATION OF INTERACTION SKILLS

Generalization here is defined as the policy’s ability to execute consistent interactions while adapting to variations in the state of the interacting object. A foundation for such generalization is accurate interaction imitation. To prevent overfitting to the specific trajectories in the demonstration, the student policy does not receive phase or reference data as observations. Beyond this, robust generalization is achieved through three complementary mechanisms: (1) Diverse offline data from XGen, which covers a broad distribution of object states; (2) Online augmentation via disturbed initialization during training, which further expands state coverage; and (3) Interaction-aware termination, which prioritizes interaction success and discourages overfitting to body motion alone. As a result, the skills acquired by HumanX extend far beyond sim-

ple motion replay. For example, from a single video demonstration, the policy learns to execute sustained human–robot basketball passing for over ten consecutive cycles.

VI. EXPERIMENTS

We conduct comprehensive experiments to evaluate the effectiveness of our method. The evaluation comprises two parts: simulation experiments on three representative interaction skills, and real-world deployment experiments covering five distinct domains with a total of ten different skills.

A. Experimental Settings

Video clips for XGen was captured using an iPhone 16. All training and simulation were conducted on the Isaac Gym platform [30] using a single NVIDIA RTX 4090 GPU with 16,384 parallel environments. Each policy was trained for 20,000 iterations unless otherwise specified.

Deployment was performed on a Unitree G1 humanoid robot. For MoCap-based experiments, we employed a Noitom optical motion capture system within a $5 \times 5 \times 2.6$ m space, using 14 cameras. The policy and mocap systems ran at 100 Hz, while the low-level PD controller operated at 1000 Hz.

B. Simulation Experiments

1) *Main Evaluation and Ablation Study*: To evaluate the effectiveness of our method and compare it with existing approaches, we conduct simulation experiments on three representative interaction tasks: (1) *Basketball Catch-Shot*: catching a passed basketball and shooting it into a target hoop. Success is defined as the shot landing within 20 cm of the target hoop center. (2) *Badminton Hitting*: striking a flying shuttlecock, with success measured by the hitting rate. (3) *Cargo Pickup*: walking to and lifting a randomly placed cargo. Success requires the lifted cargo to reach within 10 cm of the target height. We perform a series of ablation studies on our method, starting from our baseline (XMimic Base), and incrementally add: disturbed initialization (+DI), interaction termination (+IT), XGen data augmentation (+Data Aug), and the teacher-student scheme (+Tea-Stu). For comparison, we also evaluate on existing HOI imitation methods including SkillMimic [50], OmniRetarget [58], and HDMI [52].

For each task, a single video demonstration is processed by XGen to generate one training clip. In the “+Data Aug” and “+Tea-Stu” settings, the demonstration is augmented by XGen to produce 50 interaction clips for training.

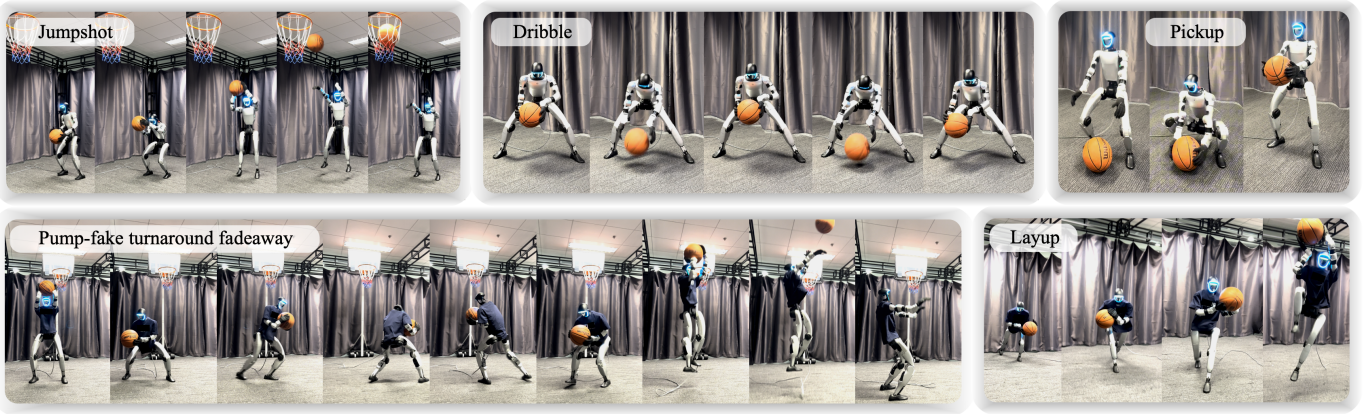


Fig. 9: Real Robot Experiment on Blind Basketball Skills. The proposed method fully leverages proprioception to control objects and enables diverse, highly dynamic, and complex interactions without any explicit object perception.

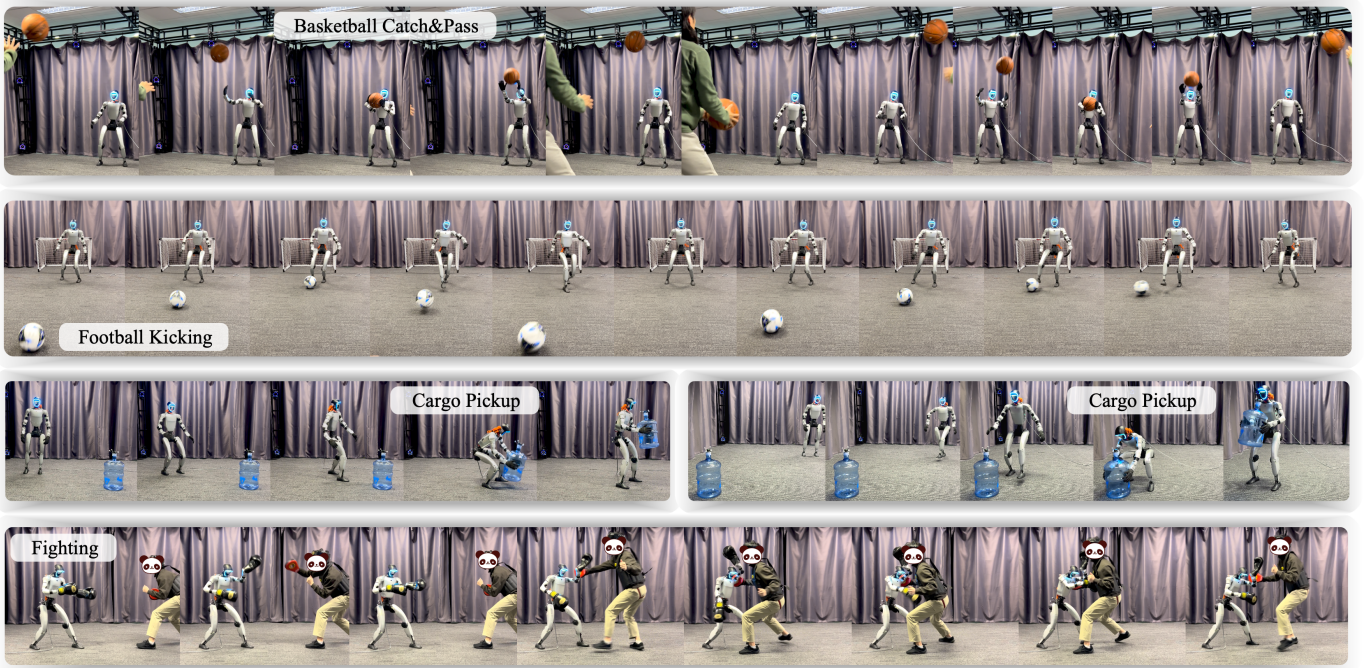


Fig. 10: Real Robot Experiment on MoCap-based Interaction Skills. When utilizing MoCap system to perceive object or human motion, our method enables sustained interaction, demonstrating high precision, agility, robustness, and generalization capability. Notably, each task shown here is learned from a single demonstration video without any task-specific reward.

We report four metrics: (1) object-position error on the original demonstration (E_o), (2) key-body-position error on the original demonstration (E_h), (3) success rate (SR) on the original demonstration, and (4) SR within a specified generalization range (GSR). For GSR, the test cases are sampled from the augmented distribution. For Basketball Catch-and-Shot, the ball's initial position is perturbed by $\pm 0.3m$ (uniform distribution). This creates novel passing trajectories and requires shooting to a new target hoop location simultaneously. For Badminton Hitting, the shuttlecock's initial position is perturbed by $\pm 0.3m$ (uniform distribution). For Cargo Pickup, the object is randomly placed within a semicircular area of $3m$ radius in front of the robot's initial orientation.

Quantitative results are summarized in Tab. I. SkillMimic

and OmniRetarget exhibit unsatisfactory performance across all three skills. While HDMI achieves reasonable success rates on two skills, its generalization capability remains limited. In contrast, our method consistently delivers near-perfect SR in the base setting, alongside superior performance on other metrics, indicating that our reward design enables more accurate and robust interaction imitation. Subsequent ablation studies highlight significant gains in GSR, with our final model exceeding 80% average GSR—approximately 8x higher than HDMI. A slight decrease in SR on certain tasks can be attributed to the reduced overfitting to the single demonstration, which is a natural trade-off when learning generalizable skills. Fig. 6 illustrates simulated executions of our generalized catch-and-shot skill. Fig. 8 visualizes the generalization ranges

TABLE II: Evaluation on Multi-Pattern Interaction Skills in Simulation. Each skill contains three distinct interaction patterns.

Method	<i>Football Kicking</i>	<i>Badminton Hitting</i>
w/o Tea-Stu	74.2% GSR	52.4% GSR
w/ Tea-Stu	93.1% GSR	84.3% GSR

TABLE III: Quantitative Results on Real Robot Experiments.

Skills	SR	Skills	SR
<i>Basketball Catch-Pass</i> (MoCap)	41 / 50	<i>Jumpshot</i> (NEP)	8 / 10
<i>Cargo Pickup</i> (MoCap)	43 / 50	<i>Dribble</i> (NEP)	8 / 10
<i>Football Kicking</i> (MoCap)	42 / 50	<i>Pump-fake</i> (NEP)	9 / 10
<i>Reactive Fighting</i> (MoCap)	37 / 50	<i>Layup</i> (NEP)	7 / 10
<i>Basketball Pickup</i> (NEP)	10 / 10	<i>Spin Move</i> (NEP)	9 / 10

for each skill. Notably, this strong generalization capability is learned from only a single demonstration video per skill.

2) *Evaluation on Multi-Pattern Interaction Skills:* To assess whether a single student policy can learn diverse skill patterns, we test on two representative tasks: *Football Kicking* and *Badminton Hitting*. For each task, three distinct human demonstration videos are processed by XGen and augmented for training. An ablation study confirms the critical role of the teacher-student scheme in this setting. Quantitative and qualitative results (Tab. II and Fig. 7) show that XMimic successfully learns multiple patterns, with the teacher-student framework yielding greater benefits in multi-pattern learning than in single-pattern scenarios.

C. Real Robot Experiments

We evaluate real-world deployment under two perception schemes: *NEP mode* (no external sensors) and *MoCap mode* (real-time object poses provided by a MoCap system). Each skill is trained based on a single video.

1) *NEP Mode:* We test five basketball skills in NEP mode: *Jumpshot*, *Dribble*, *Pickup*, *Layup*, and *Pump-fake turnaround fadeaway*. Each skill starts with the ball in hand (or on the floor for Pickup). A trial is successful if the robot completes the entire sequence without dropping the ball and remains balanced. Over 10 trials per skill (Tab. III), the policy achieves high success rates, demonstrating reliable proprioceptive control for diverse interaction behaviors (Fig. 9).

2) *MoCap Mode:* We evaluate four interactive tasks using MoCap: *Cargo Pickup*, sustained *Basketball Catch-and-Pass* and *Football Kicking* with a human partner, and *Reactive Fighting* (blocking and countering human punches). Success rates over 50 trials per skill are reported in Tab. III.

Our method enables prolonged, closed-loop interaction. For instance, in basketball, the robot can execute over 10 consecutive successful catch-and-pass cycles with a human partner, maintaining stability even if the ball is dropped and seamlessly resuming when the ball is returned. Similarly, in football, it achieves over 14 consecutive successful return kicks despite variability in human passes. This consistent performance under



Fig. 11: Emergent Behaviors. During the execution of the Cargo Pickup skill, a researcher first kicks the robot forcefully, then takes the object from its hand and places it on the ground. The robot demonstrates robust adaptation in response to such complex disturbances.

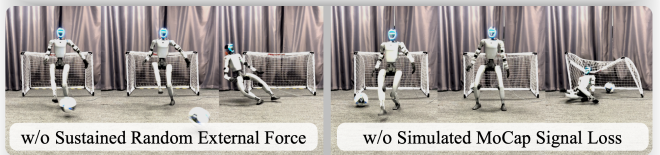


Fig. 12: Sim-to-Real Analysis. (Left) If the training does not include sustained random external forces, the robot may lose balance during highly dynamic interactions. (Right) Without simulating MoCap signal loss during training, the robot may collapse when the object signal is temporarily lost during deployment.

human-induced uncertainty strongly evidences the policy’s generalization capability.

The learned skills exhibit a high degree of autonomy and interesting emergent recovery behaviors. As shown in Fig. 11, during cargo pickup, the robot maintains a stable grasp while compensating for external pushes. If the object is taken and placed elsewhere, the robot autonomously walks to it and picks it up again. In the fighting task, the robot distinguishes between feints and genuine attacks—reacting to a pretend punch with a brief, human-like startle but reserving full defensive and counter maneuvers only for real strikes. The results visualized in Fig. 10 demonstrate that the acquired skills extend far beyond simple mimicry. They show adaptive closed-loop execution, robustness to perturbations, and the ability to generalize within interactive scenarios, confirming the effectiveness of our HumanX system. Finally, Fig. 12 illustrates two key factors critical for deployment stability.

VII. CONCLUSION

This paper presents HumanX, a full-stack framework that compiles monocular human video into agile and generalizable interaction skills for humanoids without task-specific rewards. HumanX integrates two synergistic components: XGen, which synthesizes and augments physically plausible interaction data from video, and XMimic, a unified imitation-learning framework that trains robust policies. Evaluated across 10 skills in five domains—from basketball to reactive fighting—our method achieves over 8× higher generalization success than prior approaches. On a Unitree G1 robot, HumanX enables both perception-free execution of complex maneuvers (e.g., pump-fake turnaround fadeaways) and sustained closed-loop interactions (e.g., over 10 consecutive human-robot passes), demonstrating a scalable, task-agnostic pathway for acquiring real-world interactive skills from human video.

REFERENCES

[1] Arthur Allshire, Hongsuk Choi, Junyi Zhang, David McAllister, Anthony Zhang, Chung Min Kim, Trevor Darrell, Pieter Abbeel, Jitendra Malik, and Angjoo Kanazawa. Visual imitation enables contextual humanoid control. *arXiv preprint arXiv:2505.03729*, 2025.

[2] Joao Pedro Araujo, Yanjie Ze, Pei Xu, Jiajun Wu, and C. Karen Liu. Retargeting matters: General motion retargeting for humanoid motion tracking. *arXiv preprint arXiv:2510.02252*, 2025.

[3] Qingwei Ben, Feiyu Jia, Jia Zeng, Junting Dong, Dahua Lin, and Jiangmiao Pang. Homie: Humanoid loco-manipulation with isomorphic exoskeleton cockpit. *ArXiv*, abs/2502.13013, 2025.

[4] Johan Bjorck, Fernando Castañeda, Nikita Cherniadev, Xingye Da, Runyu Ding, Linxi Fan, Yu Fang, Dieter Fox, Fengyuan Hu, Spencer Huang, et al. Gr0ot n1: An open foundation model for generalist humanoid robots. *arXiv preprint arXiv:2503.14734*, 2025.

[5] Xingyu Chen, Fu-Jen Chu, Pierre Gleize, Kevin J Liang, Alexander Sax, Hao Tang, Weiyao Wang, Michelle Guo, Thibaut Hardin, Xiang Li, et al. Sam 3d: 3dfy anything in images. *arXiv preprint arXiv:2511.16624*, 2025.

[6] Zixuan Chen, Mazeyu Ji, Xuxin Cheng, Xuanbin Peng, Xue Bin Peng, and Xiaolong Wang. Gmt: General motion tracking for humanoid whole-body control. *arXiv preprint arXiv:2506.14770*, 2025.

[7] Xuxin Cheng, Yandong Ji, Junming Chen, Ruihan Yang, Ge Yang, and Xiaolong Wang. Expressive whole-body control for humanoid robots. *arXiv preprint arXiv:2402.16796*, 2024.

[8] Xuxin Cheng, Jialong Li, Shiqi Yang, Ge Yang, and Xiaolong Wang. Open-television: Teleoperation with immersive active visual feedback. In *Conference on Robot Learning*, pages 2729–2749. PMLR, 2025.

[9] Roy Featherstone. *Rigid body dynamics algorithms*. Springer, 2008.

[10] Zipeng Fu, Qingqing Zhao, Qi Wu, Gordon Wetzstein, and Chelsea Finn. Humanplus: Humanoid shadowing and imitation from humans. *arXiv preprint arXiv:2406.10454*, 2024.

[11] Tuomas Haarnoja, Ben Moran, Guy Lever, Sandy H. Huang, Dhruva Tirumala, Markus Wulfmeier, Jan Humprik, Saran Tunyasuvunakool, Noah Siegel, Roland Hafner, Michael Bloesch, Kristian Hartikainen, Arunkumar Byravan, Leonard Hasenclever, Yuval Tassa, Fereshteh Sadeghi, Nathan Batchelor, Federico Casarini, Stefano Saliceti, Charles Game, Neil Sreendra, Kushal Patel, Marlon Gwira, Andrea Huber, Nicole Hurley, Francesco Nori, Raia Hadsell, and Nicolas Manfred Otto Heess. Learning agile soccer skills for a bipedal robot with deep reinforcement learning. *Science Robotics*, 9, 2023.

[12] Yana Hasson, Gü̈l Varol, Dimitrios Tzionas, Igor Kalevatykh, Michael J. Black, Ivan Laptev, and Cordelia Schmid. Learning joint reconstruction of hands and manipulated objects. In *2019 IEEE/CVF Conference on Computer Vision and Pattern Recognition (CVPR)*, pages 11799–11808, 2019.

[13] Tairan He, Zhengyi Luo, Xialin He, Wenli Xiao, Chong Zhang, Weinan Zhang, Kris Kitani, Changliu Liu, and Guanya Shi. Omnih2o: Universal and dexterous human-to-humanoid whole-body teleoperation and learning. *arXiv preprint arXiv:2406.08858*, 2024.

[14] Tairan He, Jiawei Gao, Wenli Xiao, Yuanhang Zhang, Zi Wang, Jiashun Wang, Zhengyi Luo, Guanqi He, Nikhil Sobanbab, Chaoyi Pan, et al. Asap: Aligning simulation and real-world physics for learning agile humanoid whole-body skills. *arXiv preprint arXiv:2502.01143*, 2025.

[15] Xialin He, Runpei Dong, Zixuan Chen, and Saurabh Gupta. Learning getting-up policies for real-world humanoid robots. *ArXiv*, abs/2502.12152, 2025.

[16] Nicolas Heess, Dhruva Tb, Srinivasan Sriram, Jay Lemmon, Josh Merel, Greg Wayne, Yuval Tassa, Tom Erez, Ziyu Wang, SM Eslami, et al. Emergence of locomotion behaviours in rich environments. *arXiv preprint arXiv:1707.02286*, 2017.

[17] Tao Huang, Junli Ren, Huayi Wang, Zirui Wang, Qingwei Ben, Muning Wen, Xiao Chen, Jianan Li, and Jiangmiao Pang. Learning humanoid standing-up control across diverse postures. *ArXiv*, abs/2502.08378, 2025.

[18] Tao Huang, Huayi Wang, Junli Ren, Kangning Yin, Zirui Wang, Xiao Chen, Feiyu Jia, Wentao Zhang, Junfeng Long, Jingbo Wang, et al. Towards adaptable humanoid control via adaptive motion tracking. *arXiv preprint arXiv:2510.14454*, 2025.

[19] Mazeyu Ji, Xuanbin Peng, Fangchen Liu, Jialong Li, Ge Yang, Xuxin Cheng, and Xiaolong Wang. Exbody2: Advanced expressive humanoid whole-body control. *arXiv preprint arXiv:2412.13196*, 2024.

[20] Jialong Li, Xuxin Cheng, Tianshu Huang, Shiqi Yang, Ri-Zhao Qiu, and Xiaolong Wang. Amo: Adaptive motion optimization for hyper-dexterous humanoid whole-body control. *arXiv preprint arXiv:2505.03738*, 2025.

[21] Yitang Li, Yuanhang Zhang, Wenli Xiao, Chaoyi Pan, Haoyang Weng, Guanqi He, Tairan He, and Guanya Shi. Hold my beer: Learning gentle humanoid locomotion and end-effector stabilization control. In *RSS 2025 Workshop on Whole-body Control and Bimanual Manipulation: Applications in Humanoids and Beyond*.

[22] Yixuan Li, Yutang Lin, Jieming Cui, Tengyu Liu, Wei Liang, Yixin Zhu, and Siyuan Huang. Clone: Closed-loop whole-body humanoid teleoperation for long-horizon tasks. *arXiv preprint arXiv:2506.08931*, 2025.

[23] Zhongyu Li, Xuxin Cheng, Xue Bin Peng, Pieter Abbeel, Sergey Levine, Glen Berseth, and Koushil Sreenath. Reinforcement learning for robust parameterized locomotion control of bipedal robots. In *2021 IEEE International Conference on Robotics and Automation (ICRA)*, pages 2811–2817. IEEE, 2021.

[24] Zhongyu Li, Xue Bin Peng, Pieter Abbeel, Sergey Levine, Glen Berseth, and Koushil Sreenath. Reinforcement learning for versatile, dynamic, and robust bipedal locomotion control. *The International Journal of Robotics Research*, 44(5):840–888, 2025.

[25] Qiayuan Liao, Takara E Truong, Xiaoyu Huang, Guy Tevet, Koushil Sreenath, and C Karen Liu. Beyondmimic: From motion tracking to versatile humanoid control via guided diffusion. *arXiv preprint arXiv:2508.08241*, 2025.

[26] Tengyu Liu, Zeyu Liu, Ziyuan Jiao, Yixin Zhu, and Song-Chun Zhu. Synthesizing diverse and physically stable grasps with arbitrary hand structures using differentiable force closure estimator. *IEEE Robotics and Automation Letters*, 7(1):470–477, 2021.

[27] Matthew Loper, Naureen Mahmood, Javier Romero, Gerard Pons-Moll, and Michael J. Black. Smpl: A skinned multi-person linear model. *Seminal Graphics Papers: Pushing the Boundaries, Volume 2*, 2023.

[28] Zhengyi Luo, Jinkun Cao, Kris Kitani, Weipeng Xu, et al. Perpetual humanoid control for real-time simulated avatars. In *Proceedings of the IEEE/CVF International Conference on Computer Vision*, pages 10895–10904, 2023.

[29] Yuntao Ma, Andrei Cramariuc, Farbod Farshidian, and Marco Hutter. Learning coordinated badminton skills for legged manipulators. *Science robotics*, 10 102:eadu3922, 2025.

[30] Viktor Makoviychuk, Lukasz Wawrzyniak, Yunrong Guo, Michelle Lu, Kier Storey, Miles Macklin, David Hoeller, Nikita Rudin, Arthur Allshire, Ankur Handa, and Gavriel State. Isaac gym: High performance GPU based physics simulation for robot learning. In *Thirty-fifth Conference on Neural Information Processing Systems Datasets and Benchmarks Track (Round 2)*, 2021.

[31] Richard M Murray, Zexiang Li, and S Shankar Sastry. *A mathematical introduction to robotic manipulation*. CRC press, 2017.

[32] Yixuan Pan, Ruoyi Qiao, Li Chen, Kashyap Chitta, Liang Pan, Haoguang Mai, Qingwen Bu, Hao Zhao, Cunyuan Zheng, Ping Luo, et al. Agility meets stability: Versatile humanoid control with heterogeneous data. *arXiv preprint arXiv:2511.17373*, 2025.

[33] Xue Bin Peng, Pieter Abbeel, Sergey Levine, and Michiel van de Panne. Deepmimic. *ACM Transactions on Graphics*, page 1–14, Aug 2018. doi: 10.1145/3197517.3201311.

[34] Xue Bin Peng, Angjoo Kanazawa, Jitendra Malik, Pieter Abbeel, and Sergey Levine. Sfv: Reinforcement learning of physical skills from videos. *ACM Transactions On Graphics (TOG)*, 37(6):1–14, 2018.

[35] Xue Bin Peng, Ze Ma, Pieter Abbeel, Sergey Levine, and Angjoo Kanazawa. Amp: Adversarial motion priors for stylized physics-based character control. *ACM Transactions on Graphics*, page 1–20, Aug 2021. doi: 10.1145/3450626.3459670.

[36] Junli Ren, Junfeng Long, Tao Huang, Huayi Wang, Zirui Wang, Feiyu Jia, Wentao Zhang, Jingbo Wang, Ping Luo, and Jiangmiao Pang. Humanoid goalkeeper: Learning from position conditioned task-motion constraints. *arXiv preprint arXiv:2510.18002*, 2025.

[37] John Schulman, Filip Wolski, Prafulla Dhariwal, Alec Radford, and Oleg Klimov. Proximal policy optimization algorithms. *arXiv preprint arXiv:1707.06347*, 2017.

[38] Yiyang Shao, Xiaoyu Huang, Bike Zhang, Qiayuan Liao, Yuman Gao, Yufeng Chi, Zhongyu Li, Sophia Shao, and Koushil Sreenath. Langwbc: Language-directed humanoid whole-body control via end-to-end learning. *ArXiv*, abs/2504.21738, 2025.

[39] Zehong Shen, Huaijin Pi, Yan Xia, Zhi Cen, Sida Peng, Zechen Hu, Hujun Bao, Ruizhen Hu, and Xiaowei Zhou. World-grounded human motion recovery via gravity-view coordinates. In *SIGGRAPH Asia Conference Proceedings*, 2024.

[40] Zhi Su, Bike Zhang, Nima Rahmanian, Yuman Gao, Qiayuan Liao, Caitlin Regan, Koushil Sreenath, and S Shankar Sastry. Hitter: A humanoid table tennis robot via hierarchical planning and learning. *arXiv preprint arXiv:2508.21043*, 2025.

[41] Jiaming Sun, Zihao Wang, Siyu Zhang, Xingyi He He, Hongcheng Zhao, Guofeng Zhang, and Xiaowei Zhou. Onepose: One-shot object pose estimation without cad models. In *2022 IEEE/CVF Conference on Computer Vision and Pattern Recognition (CVPR)*, pages 6815–6824, 2022.

[42] Russ Tedrake, Teresa Weirui Zhang, and H Sebastian Seung. Stochastic policy gradient reinforcement learning on a simple 3d biped. In *2004 IEEE/RSJ International Conference on Intelligent Robots and Systems (IROS)(IEEE Cat. No. 04CH37566)*, volume 3, pages 2849–2854. IEEE, 2004.

[43] Chen Tessler, Yifeng Jiang, Erwin Coumans, Zhengyi Luo, Gal Chechik, and Xue Bin Peng. Maskedmanipulator: Versatile whole-body control for loco-manipulation. *arXiv preprint arXiv:2505.19086*, 2025.

[44] Josh Tobin, Rachel Fong, Alex Ray, Jonas Schneider, Wojciech Zaremba, and Pieter Abbeel. Domain randomization for transferring deep neural networks from simulation to the real world. In *2017 IEEE/RSJ international conference on intelligent robots and systems (IROS)*, pages 23–30. IEEE, 2017.

[45] Huayi Wang, Zirui Wang, Junli Ren, Qingwei Ben, Tao Huang, Weinan Zhang, and Jiangmiao Pang. Beamdojo: Learning agile humanoid locomotion on sparse footholds. *ArXiv*, abs/2502.10363, 2025.

[46] Huayi Wang, Wentao Zhang, Runyi Yu, Tao Huang, Junli Ren, Feiyu Jia, Zirui Wang, Xiaojie Niu, Xiao Chen, Jiahe Chen, et al. Phyhsit: Towards a real-world generalizable and natural humanoid-scene interaction system. *arXiv preprint arXiv:2510.11072*, 2025.

[47] Ruicheng Wang, Jialiang Zhang, Jiayi Chen, Yinzhen Xu, Puha Li, Tengyu Liu, and He Wang. Dexgrasp-

net: A large-scale robotic dexterous grasp dataset for general objects based on simulation. *arXiv preprint arXiv:2210.02697*, 2022.

[48] Yinhuai Wang, Jing Lin, Ailing Zeng, Zhengyi Luo, Jian Zhang, and Lei Zhang. Physhoi: Physics-based imitation of dynamic human-object interaction. *arXiv preprint arXiv:2312.04393*, 2023.

[49] Yinhuai Wang, Runyi Yu, Hok Wai Tsui, Xiaoyi Lin, Hui Zhang, Qihan Zhao, Ke Fan, Miao Li, Jie Song, Jingbo Wang, Qifeng Chen, and Ping Tan. Learning generalizable hand-object tracking from synthetic demonstrations. *arXiv preprint arXiv:2512.19583*, 2025.

[50] Yinhuai Wang, Qihan Zhao, Runyi Yu, Hok Wai Tsui, Ailing Zeng, Jing Lin, Zhengyi Luo, Jiwen Yu, Xiu Li, Qifeng Chen, et al. Skillmimic: Learning basketball interaction skills from demonstrations. In *Proceedings of the Computer Vision and Pattern Recognition Conference*, pages 17540–17549, 2025.

[51] Bowen Wen, Wei Yang, Jan Kautz, and Stanley T. Birchfield. Foundationpose: Unified 6d pose estimation and tracking of novel objects. *2024 IEEE/CVF Conference on Computer Vision and Pattern Recognition (CVPR)*, pages 17868–17879, 2023.

[52] Haoyang Weng, Yitang Li, Nikhil Sobanbabu, Zihan Wang, Zhengyi Luo, Tairan He, Deva Ramanan, and Guanya Shi. Hdmi: Learning interactive humanoid whole-body control from human videos. *arXiv preprint arXiv:2509.16757*, 2025.

[53] Weiji Xie, Jinrui Han, Jiakun Zheng, Huanyu Li, Xinzhe Liu, Jiyuan Shi, Weinan Zhang, Chenjia Bai, and Xuelong Li. Kungfubot: Physics-based humanoid whole-body control for learning highly-dynamic skills. *arXiv preprint arXiv:2506.12851*, 2025.

[54] Pei Xu, Xumin Shang, Victor Zordan, and Ioannis Karamouzas. Composite motion learning with task control. *ACM Transactions on Graphics (TOG)*, 42(4):1–16, 2023.

[55] Pei Xu, Zhen Wu, Ruocheng Wang, Vishnu Sarukkai, Kayvon Fatahalian, Ioannis Karamouzas, Victor B Zordan, and C. Karen Liu. Learning to ball: Composing policies for long-horizon basketball moves. *ACM Transactions on Graphics (TOG)*, 44:1 – 14, 2025.

[56] Sirui Xu, Hung Yu Ling, Yu-Xiong Wang, and Liang-Yan Gui. Intermimic: Towards universal whole-body control for physics-based human-object interactions. *arXiv preprint arXiv:2502.20390*, 2025.

[57] Yufei Xue, Wentao Dong, Minghuan Liu, Weinan Zhang, and Jiangmiao Pang. A unified and general humanoid whole-body controller for fine-grained locomotion. *ArXiv*, abs/2502.03206, 2025.

[58] Lujie Yang, Xiaoyu Huang, Zhen Wu, Angjoo Kanazawa, Pieter Abbeel, Carmelo Sferrazza, C Karen Liu, Rocky Duan, and Guanya Shi. Omniretarget: Interaction-preserving data generation for humanoid whole-body loco-manipulation and scene interaction. *arXiv preprint arXiv:2509.26633*, 2025.

[59] Kangning Yin, Weishuai Zeng, Ke Fan, Minyue Dai, Zirui Wang, Qiang Zhang, Zheng Tian, Jingbo Wang, Jiangmiao Pang, and Weinan Zhang. Unitracker: Learning universal whole-body motion tracker for humanoid robots. *arXiv preprint arXiv:2507.07356*, 2025.

[60] Runyi Yu, Yinhuai Wang, Qihan Zhao, Hok Wai Tsui, Jingbo Wang, Ping Tan, and Qifeng Chen. Skillmimic-v2: Learning robust and generalizable interaction skills from sparse and noisy demonstrations. In *Proceedings of the Special Interest Group on Computer Graphics and Interactive Techniques Conference Conference Papers*, pages 1–11, 2025.

[61] Yanjie Ze, Zixuan Chen, Joao Pedro Araújo, Zi-ang Cao, Xue Bin Peng, Jiajun Wu, and C Karen Liu. Twist: Teleoperated whole-body imitation system. *arXiv preprint arXiv:2505.02833*, 2025.

[62] Weishuai Zeng, Shunlin Lu, Kangning Yin, Xiaojie Niu, Minyue Dai, Jingbo Wang, and Jiangmiao Pang. Behavior foundation model for humanoid robots. *arXiv preprint arXiv:2509.13780*, 2025.

[63] Chong Zhang, Wenli Xiao, Tairan He, and Guanya Shi. Wococo: Learning whole-body humanoid control with sequential contacts. In *Conference on Robot Learning*, pages 455–472. PMLR, 2025.

[64] Haotian Zhang, Ye Yuan, Viktor Makoviychuk, Yunrong Guo, Sanja Fidler, Xue Bin Peng, and Kayvon Fatahalian. Learning physically simulated tennis skills from broadcast videos. *ACM Trans. Graph.*, 2023. doi: 10.1145/3592408.

[65] Zhikai Zhang, Jun Guo, Chao Chen, Jilong Wang, Chenghuai Lin, Yunrui Lian, Han Xue, Zhenrong Wang, Maoqi Liu, Jiangran Lyu, et al. Track any motions under any disturbances. *arXiv preprint arXiv:2509.13833*, 2025.

[66] Ziwen Zhuang, Shenzhe Yao, and Hang Zhao. Humanoid parkour learning. *arXiv preprint arXiv:2406.10759*, 2024.

TABLE IV: Observation and Reward Settings. *: optional.

Observations			Rewards		
Curr Terms	π_{tea}	π_{stu}	Mimic Terms	π_{tea} & π_{stu}	
Base Ang Vel	✓	✓	Body Pos	✓	
Gravity	✓	✓	Body Rot	✓	
DoF Pos	✓	✓	Body Vel	✓	
DoF Vel	✓	✓	Body Ang Vel	✓	
Action	✓	✓	Body AMP	✓	
PD Error	✓	✓	DoF Pos	✓	
Ref Body Pos	✓		DoF Vel	✓	
Delta Body Pos	✓		Relative Motion	✓	
Object Pos	✓	*	Object Pos	✓	
Object Rot	*	*	Object Rot	*	
Target Object Pos	*	*	Contact Graph	✓	
Target Object Rot	*	*	Reg Terms		
Skill Label		✓	Torque	✓	
History	✓	✓	Action Rate	✓	
History Terms			Waist DoF	✓	
Base Ang Vel	✓	✓	Feet Orientation	✓	
Gravity	✓	✓	Feet Slippage	✓	
DoF Pos	✓	✓	DoF Limit	✓	
DoF Vel	✓	✓	Torque Limit	✓	
Action	✓	✓	Termination	✓	

VIII. UNIFIED INTERACTION IMITATION REWARD

To enable the humanoid to accurately imitate the interactions present in the reference data, we employ the following composite reward function:

$$r_t = r_t^{\text{body}} + r_t^{\text{obj}} + r_t^{\text{rel}} + r_t^c + r_t^{\text{reg}}, \quad (5)$$

where r_t^{body} is the body imitation reward, r_t^{obj} is the object imitation reward, r_t^{rel} encourages correct relative motion between the body and the object, r_t^c is the contact imitation reward, and r_t^{reg} comprises several regularization and penalty terms to improve motion stability. Tab. IV provides a summary.

1) *Body Motion Imitation Reward*: The body reward is decomposed into multiple tracking terms:

$$r_t^{\text{body}} = r_t^p + r_t^r + r_t^d + r_t^v + r_t^{rv} + r_t^{dv} + r_t^{\text{amp}}. \quad (6)$$

These terms correspond to body position, body rotation, joint position (DoF), body linear velocity, body angular velocity, and joint velocity, respectively. The adversarial motion prior (AMP) reward [35] is effective in enhancing the smoothness and naturalness of the body motion. Each sub-reward except r_t^{amp} follows the general form:

$$r_t^\alpha = \gamma^\alpha \cdot \exp(-\lambda^\alpha \cdot e_t^\alpha), \quad (7)$$

where e_t^α denotes the imitation error for modality α at time t , λ^α and γ^α are weight and sensitivity hyperparameter.

2) *Object Motion Imitation Reward*: The object reward ensures accurate tracking of the object’s state:

$$r_t^{\text{obj}} = r_t^{op} + r_t^{or}, \quad (8)$$

where r_t^{op} and r_t^{or} (optional) are the object position and rotation imitation rewards, respectively. Both are computed using the formulation in Eq. (7).

3) *Body-Object Relative Motion Imitation Reward*: The relative motion reward consists of two terms:

$$r_t^{\text{rel}} = r_t^{\text{rel_p}} + r_t^{\text{rel_r}}, \quad (9)$$

where $r_t^{\text{rel_p}}$ encourages correct relative positioning and $r_t^{\text{rel_r}}$ (optional) encourages correct relative orientation between the body and the object. Both follow the same form as Eq. (7).

The relative position error is computed as

$$e_t^{\text{rel_p}} = \|\mathbf{u}_t - \hat{\mathbf{u}}_t\|_2, \quad (10)$$

where $\hat{\mathbf{u}}_t$ is the set of reference relative-position vectors, and \mathbf{u}_t is the corresponding set from the simulation. Each vector in \mathbf{u}_t is defined as $\mathbf{u}_t^{(k)} = \mathbf{u}_t^k - \mathbf{u}_t^o$, with \mathbf{u}_t^k being the 3D position of a body keypoint (e.g., left middle fingertip) and \mathbf{u}_t^o the object position. The relative rotation error is given by

$$e_t^{\text{rel_r}} = \sum_k d(R_t^{(k)}, \hat{R}_t^{(k)}), \quad (11)$$

where $R_t^{(k)}$ denotes the rotation of the object relative to body keypoint k (i.e., $R_t^{(k)} = R_t^{\text{obj}}(R_t^{(k)-1})$), $\hat{R}_t^{(k)}$ is the corresponding reference relative rotation, and $d(\cdot, \cdot)$ is a distance metric on $\text{SO}(3)$ (e.g., the geodesic angle between two rotations). This formulation ensures that the spatial relationship between the robot and the object is accurately preserved across both translation and rotation.

4) *Contact Graph Imitation Reward*: To accurately reproduce the contact patterns present in the human demonstrations, we introduce a contact imitation reward. Our XGen pipeline annotates each frame with a contact label, indicating whether the object and key-bodies are in contact status. Similar to prior works [48, 50, 60], we formulate the contact state as a Contact Graph (CG), represented as a binary vector $s_t^{cg} \in \{0, 1\}^J$, where J is the number of contact bodies, and a value of 1 indicates active contact.

The contact reward is computed based on the discrepancy between the simulated contact state s_t^{cg} and the reference contact state \hat{s}_t^{cg} from the reference data. The contact error vector is defined as the element-wise absolute difference:

$$e_t^{cg} = |s_t^{cg} - \hat{s}_t^{cg}|.$$

The contact imitation reward is then given by an exponential of the weighted error:

$$r_t^{cg} = \exp(-\sum_{j=1}^J \lambda_j^{cg} \cdot e_t^{cg}[j]), \quad (12)$$

where λ_j^{cg} is a sensitivity weight for the j -th contact edge. This formulation penalizes mismatches in the contact graph, ensuring the policy learns precise contact timing and location.

IX. PERCEIVING EXTERNAL FORCE FROM PROPRIOCEPTION

Even in the absence of visual input, humans can still effectively perform stable grasping, basketball shooting, and other interactive behaviors. This ability relies on the implicit

perception of interaction states through tactile and force feedback. In the following, we conduct a theoretical analysis to demonstrate that a similar mechanism is also feasible for humanoid robots, identify the key variables that influence such perception, and accordingly guide the observation design.

The equation of motion for a floating-base humanoid robot can be formulated as [9, 31]:

$$\boldsymbol{\tau} = \mathbf{M}(\mathbf{q})\ddot{\mathbf{q}} + \mathbf{C}(\mathbf{q}, \dot{\mathbf{q}})\dot{\mathbf{q}} + \mathbf{G}(\mathbf{q}) + \boldsymbol{\tau}_f + \mathbf{J}_{\text{ext}}^{\top} \mathbf{F}_{\text{ext}}, \quad (13)$$

where $\boldsymbol{\tau}$ denotes the vector of commanded joint torques; \mathbf{q} , $\dot{\mathbf{q}}$, and $\ddot{\mathbf{q}}$ are the joint positions, velocities, and accelerations, respectively; \mathbf{M} is the mass matrix; \mathbf{C} captures Coriolis and centrifugal terms; \mathbf{G} is the gravity vector; $\boldsymbol{\tau}_f$ accounts for joint friction; and $\mathbf{J}_{\text{ext}}^{\top} \mathbf{F}_{\text{ext}}$ represents the joint-space projection of external contact forces \mathbf{F}_{ext} . Rearranging Eq. 13 yields

$$\mathbf{J}_{\text{ext}}^{\top} \mathbf{F}_{\text{ext}} = \boldsymbol{\tau} - (\mathbf{M}\ddot{\mathbf{q}} + \mathbf{C}\dot{\mathbf{q}} + \mathbf{G} + \boldsymbol{\tau}_f). \quad (14)$$

which shows that the external forces on each joint can be estimated if corresponding parameters are available. In the context of training a whole-body control policy with RL, this implies that, in principle, a policy can possibly learn to implicitly perceive external forces—provided it is given access to the relevant observations—and thus achieve a better dynamic interaction with objects. Taking the Unitree G1 as an example, \mathbf{q} and $\dot{\mathbf{q}}$ are directly measurable, and $\boldsymbol{\tau}$ is well approximated by the commanded torque $\boldsymbol{\tau}_{\text{cmd}}$ from the PD controller. Although the joint acceleration $\ddot{\mathbf{q}}$ is not directly available, we can implicitly provide coarse acceleration information by including a history of multiple frames of $\dot{\mathbf{q}}$ in the observations. The remaining terms in Eq. 14 are approximately constant and therefore do not need to be provided to the policy.

Based on these insights, the final observation components used in our policy are listed in Tab. IV; they account (either explicitly or implicitly) for all variables appearing in Eq. 14.